Received 8 March 2026; revised 3 April 2026; accepted 7 April 2026. Date of publication 13 April 2026; date of current version 11 June 2026.

Digital Object Identifier 10.1109/OJAP.2026.3683425

Broadband and Hemispherical Coverage Characteristics of Compact and Asymmetric Dipole Array for Millimeter-Wave Portable Applications

JAE-YEONG LEE[1,2] (Member, IEEE), SHUAI ZHANG[3] (Fellow, IEEE), AND WONBIN HONG[1] (Fellow, IEEE)

[1]Department of Electrical Engineering, Pohang University of Science and Technology, Pohang 37673, South Korea
[2]X-ray·Terahertz Components Research Section, Electronics and Telecommunications Research Institute, Daejeon 34129, South Korea
[3]Department of Electronic Systems, Aalborg University, 9220 Aalborg, Denmark

CORRESPONDING AUTHORS: JAE-YEONG LEE AND WONBIN HONG (e-mail: jylee82@etri.re.kr; whong@postech.ac.kr)

This work was supported in part by the Basic Science Research Program through the National Research Foundation (NRF) of Korea funded by the Ministry of Education under Grant 2021R1I1A1A01057159; in part by the Next Generation Engineering Research Program of NRF of Korea funded by Ministry of Science, Information and Communication Technology (MSIT) under Grant 2019H1D8A2106519; in part by the Institute for Information and Communications Technology Planning and Evaluation (IITP) grant funded by MSIT under Grant RS-2021-II210763; and in part by Korea Planning and Evaluation Institute of Industrial Technology (KEIT) grant funded by the Ministry of Trade, Industry, and Resources (MOTIR), South Korea, under Grant RS-2024-00442865.

ABSTRACT This article presents a compact and asymmetric dipole array (CADA) fabricated on a single-layer FR-4 PCB featuring hemispherical coverage across a broadband spectrum for the millimeter-wave (mmWave) portable applications. The compensation effect between inter-element capacitance and inductance of the proposed CADA can exhibit a high coupling level based on leaky-wave radiation behavior in a 1-D linear array with $0.3\lambda_0$ spacing (@ operating lowest freq.). However, it is possible to maintain a wide impedance matching bandwidth due to the absence of balun circuitry that can limit the operating bandwidth of the antenna. To investigate the influence of compression on the proposed 8-element CADA, array antennas with different inter-element spacing and T-junction power dividers, including the predetermined phased delay in each antenna element, are designed and characterized. In addition, high-precision compensation techniques for obtaining the accurate insertion loss of the T-junction power dividers are demonstrated to estimate the directivity of the stand-alone antenna array with different inter-element spacing in three different beam-steering scenarios. Afterward, the fabricated array antennas are characterized by their radiation patterns and beam scan range within 3-dB scan loss in the frequency range from 25 to 35 GHz, and over-the-air (OTA) results. Despite the compressed element configuration without additional baluns or decoupling circuits, the proposed array, based on an extremely low-cost fabrication process, realizes hemispherical coverage in the frequency range from 25 to 35 GHz. In addition, the proposed array exhibits lower than 9% error vector magnitude (EVM) at 4.8 Gbps maximum data rates.

INDEX TERMS Millimeter-wave antenna arrays, compact antennas, end-fire antennas, broadband antennas, spherical beam coverage.

I. INTRODUCTION

TO INCREASE the coverage and spectrum efficiency in the millimeter-wave/sub-terahertz (mmWave/sub-THz) spectrum despite the physical threshold properties of active RF components, compact phased-array antenna modules have been spotlighted [1], [2], [3], [4], [5], [6]. The phased-array antenna modules consist of lots of antenna elements, beamforming IC (BFIC) chipsets, and feeding networks [3], [6], [7]. However, conventional phased-array antenna modules still suffer from a trade-off among the overall development cost, form factor, RF performance linked to materials or fabrication, and measurement techniques [6], [7], [8], [9], [10], [11]. Recently, the commercial standalone complementary metal oxide semiconductor (CMOS) BFIC chipsets featuring cost-effectiveness have been developed to realize comparable RF performance, without any usage of compound semiconductor chipsets in terms of overall figure-of-merit (FoM) [6], [11], [12], [13]. Nevertheless, to support both remarkable RF performance and cost-effectiveness within a small form factor, the phased array antenna techniques are still a key challenging issue in mmWave/sub-THz portable applications [11], [12], [13], [14], [15], [16], [17], [18], [19], [20].

The performance of phased array antennas in the mmWave/sub-THz spectrum can be deteriorated due to two critical reasons related to the fabrication process techniques and material properties [6], [7]. First, the conventional fabrication process techniques suffer from conflicting constraints, such as fabrication resolution, the number of layers, the thickness of metal and dielectric layers, reliability issues, and production cost. Second, the dielectric loss from the substrate material can be significantly increased at high frequencies. Especially, the stringent electrical properties of package material should be required due to the limitation of conventional package platforms via high insertion loss of the transmission lines in the sub-THz spectrum [16], [17]. Moreover, the antenna modules integrating with high-frequency BFIC chipsets inherently exhibit high insertion loss of feeding networks, crosstalk issues between adjacent signal paths and power paths, and various signal integrity (SI) problems [12], [13], [14], [15]. Eventually, during the verification and product quality control stages, the entire phased array antenna modules fully integrating with BFIC chipsets suffer from severe performance degradation and an unpredictable link budget due to lots of complex issues in each sub-part [8], [9], [11], [12], [13], [14], [15].

Another key issue with phased array antennas is reducing mutual coupling between adjacent elements, which ultimately improves beam-steerable scanning performance (e.g., scan loss mitigation and grating lobe suppression) across the broadband spectrum [3], [21], [22], [23]. Conventional research on achieving good scanning performance has been categorized by using conformal array configurations, array configurations with bulky high-impedance surfaces (HIS) or decoupling circuits, and pattern-reconfigurable elements that utilize additional active RF components [10], [19], [21], [22], [23], [24], [25], [26]. Recently, compact, cost-effective mmWave antennas exhibiting broadband operation have been studied using planar HIS fabricated on a single-layer FR-4 PCB, despite the absence of balun circuits [27], [28], [29], [30]. In addition, to remove any decoupling circuits, the tightly coupled dipole antennas (TCDA) in phased array applications, which feature high mutual coupling characteristics, have been actively investigated [31], [32], [33], [34]. The state-of-the-art tightly coupled dipole array (TCDA) can be categorized by two common fundamental electromagnetic characteristics: a high mutual coupling level between elements and, similarly, acts as a compact (e.g., CRLH) metamaterial 2-D array with subwavelength properties [31], [32], [33], [34], [43], [44], [45]. Nevertheless, a compact planar antenna in a 1-D linear array without baluns and decoupling circuits should be required to achieve hemispherical coverage

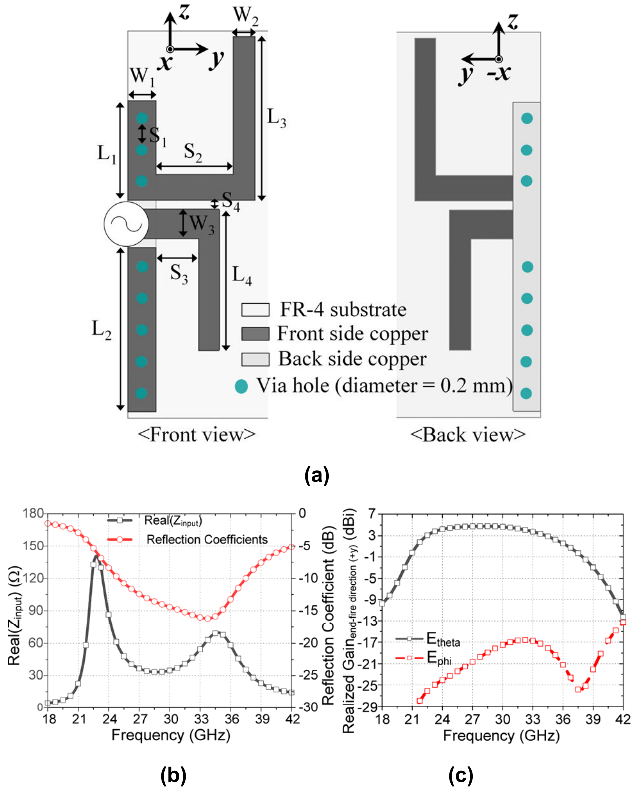

FIGURE 1. Single element of planar asymmetric dipole antenna. (a) Configuration (w_1 = 0.48 mm, w_2 = 0.36 mm, w_3 = 0.5 mm, L_1 = 1.7 mm, L_2 = L_3 = 2.8 mm, L_4 = 2.4 mm, S_1 = 0.34 mm, S_2 =1.32 mm, S_3 = 0.72 mm, S_4 =0.15 mm). (b) Simulated the real part of the input impedance and reflection coefficient. (c) Simulated realized gain toward end-fire direction (+*y*) @ two linear polarizations.

across the broadband spectrum for mmWave portable applications. Eventually, the new conceptual antenna in a 1-D linear array configuration should be investigated, exhibiting a high mutual coupling mechanism via leaky-wave behavior, with balun-free and decoupling-free.

In this work, the compact and asymmetric dipole array (CADA) concepts are presented and investigated using the cost-effective single-layer FR-4 PCB process to realize spherical coverage in the mmWave broadband spectrum and perform high-precision tests. First, the proposed CADA consists of inter-element capacitance and inductance between adjacent elements featuring a high mutual coupling level, and can be demonstrated by the coupling mechanism via leaky-wave behavior in a 1-D linear array. Moreover, due to high mutual coupling levels, the balun-free, decoupling-circuit-free, and low-loss compressed feeding networks, the proposed CADA array with the most compressed configurations can exhibit wide-angle scanning capability over an ultra-wide spectrum. Afterward, high-precision compensation techniques of insertion loss of feeding networks are demonstrated to estimate the directivity of antenna arrays for different beam steering scenarios. The fabricated antennas with different inter-element spacings for utilizing the compression effects in mmWave portable apparatus are characterized and investigated for fast and precise optimized cell coverage by comparing both measured radiation patterns

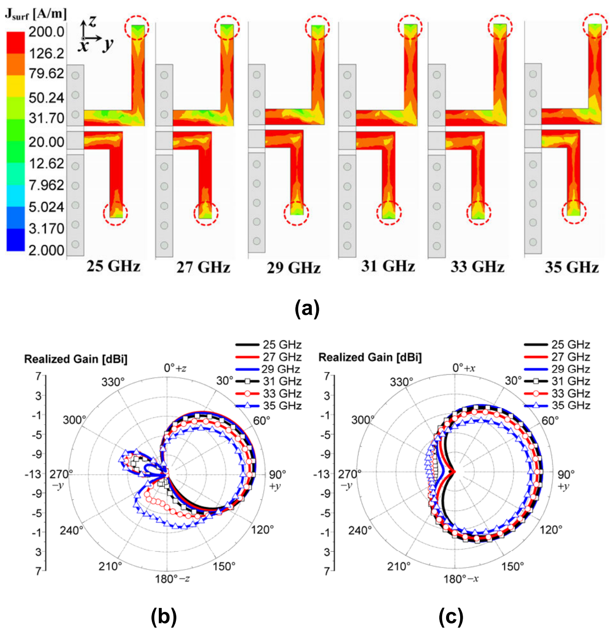

FIGURE 2. Single element of planar asymmetric dipole antenna. (a) Simulated current distributions vs. different frequencies. (b) Simulated *yz*-cut (ϕ = 90°) radiation patterns vs. different frequencies @E_{theta}-pol. (c) Simulated *xy*-cut (θ =90°) radiation patterns vs. different frequencies @E_{theta}-pol.

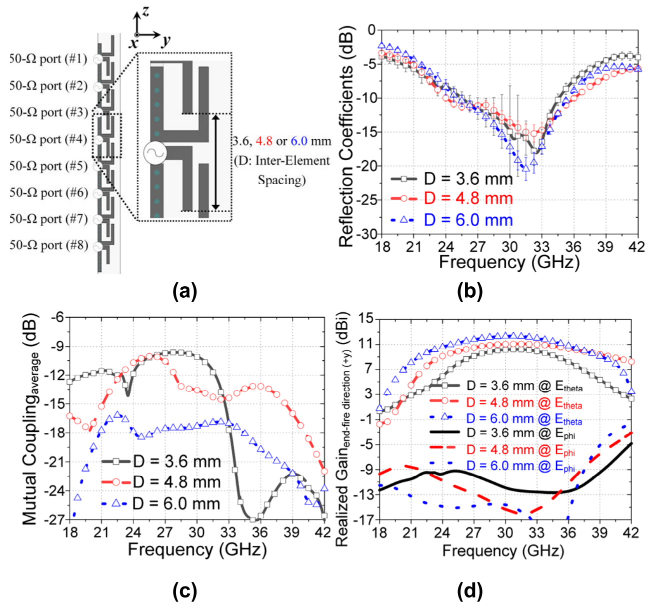

FIGURE 3. 8 Array elements with ideal 50-Ω feeding ports. (a) Configuration of array antennas with three different spacing between elements. (b) Simulated reflection coefficients (line: average value between ports, error bar: standard deviation between ports). (c) Simulated average value of mutual coupling between each adjacent port. (d) Simulated realized gain toward end-fire direction (+*y*) @ two linear polarizations.

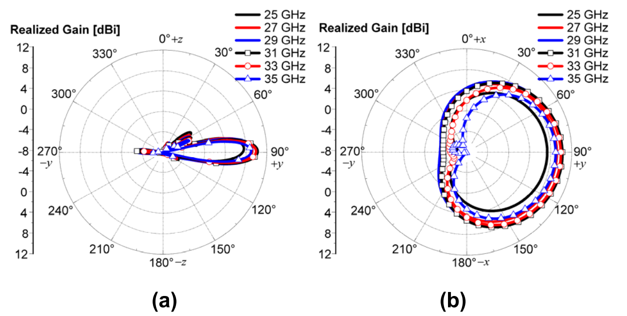

FIGURE 4. 8 Array elements of planar asymmetric dipole antenna with ideal 50-Ω feeding ports @ D= 3.6 mm (worst case of mutual coupling level). (a) Simulated *yz*-cut (ϕ =90°) vs. different frequencies @E_{theta}-pol. (b) Simulated *xy*-cut (θ = 90°)vs. different frequencies @ E_{theta}-pol.

and over-the-air (OTA) performance results at the same time [12], [13], [29], [39]. In conclusion, despite the miniaturized configuration with 3.6 mm (0.3λ_0) inter-element spacing (@ operating lowest freq.) and the absence of baluns or additional decoupling circuits, the proposed CADA arrays based on an extremely low-cost fabrication process achieve hemispherical coverage in K-/Ka-band.

II. COMPACT PHASED-ARRAY DESIGN

In this section, the compact phased array and feeding networks are designed and investigated utilizing a single element of the CADA containing T-junction power dividers with different inter-element spacings. In addition, the coupling mechanism via leaky-wave radiation behavior in the proposed 1-D CADA is also discussed in detail.

A. SINGLE ELEMENT OF COMPACT AND ASYMMETRIC DIPOLE ANTENNA

As depicted in Fig. 1(a), the proposed antenna element is integrated into a single-layer FR-4 substrate that features dimensions of 0.4 mm × 1.8 mm × 5.2 mm and a relative permittivity of 4.4. Because the input impedance of the state-of-the-art TCDA is typically above 100-Ω, bulky auxiliary feeding circuits, such as broadband impedance transformers and baluns, should be needed [31], [32], [33], [34]. However, in this work, asymmetric dipole element arms without any auxiliary feeding circuits in a single-layer FR-4 PCB are designed to induce inter-element capacitance and compensate for the inductance of dipole radiators over a broad bandwidth [33], [34], [35]. Moreover, without any auxiliary circuits, the real part of the input impedance of the proposed antenna is 35∼70-Ω in the frequency range from 25 to 35 GHz, and Fig. 1(b) illustrates the simulated real part of the input impedance of the antenna element and the simulated reflection coefficient of the antenna element.

Figs. 1(c)&2(a)-(c) present the radiation characteristics and surface current distributions of the proposed antenna across the broadband spectrum, respectively. First, the antenna acts similarly to a typical half-wavelength dipole radiation mode without any balun circuitry across the broadband spectrum, as illustrated in the current distributions of Fig. 2(a). The currents at all frequencies are along the z-direction, and peak currents around the center of the antenna are observed. Moreover, the high impedance condition at the edge positions can be checked. Second, due to the inserted-via-wall structures functioning as an effective reflector, the proposed antenna exhibits a high realized gain toward

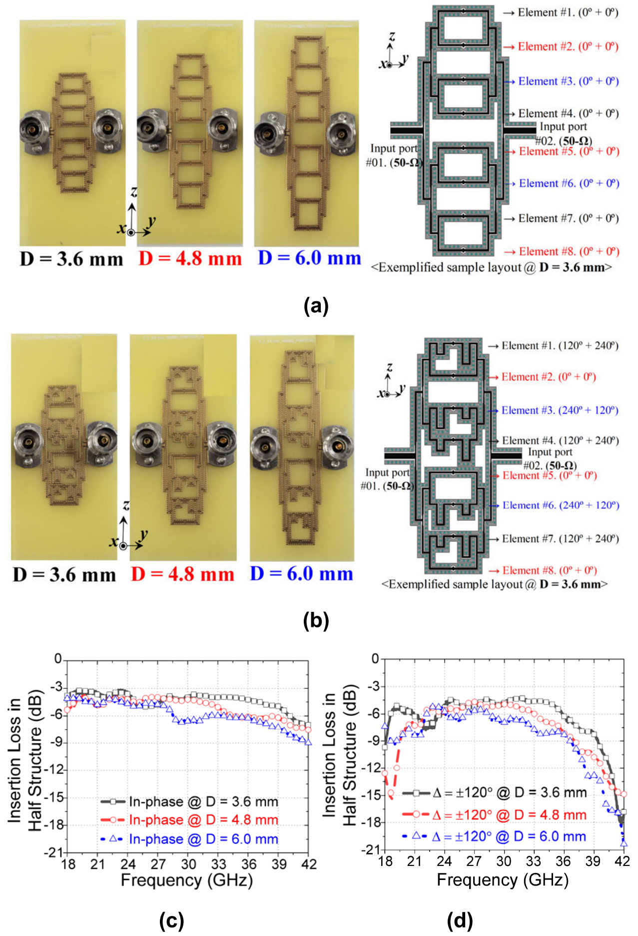

FIGURE 5. **Photograph and detailed phase mapping of a back-to-back configuration for T-junction power dividers exhibiting an in-phase difference among all elements. (b) Photograph and detailed phase mapping of a back-to-back configuration for T-junction power dividers exhibiting Δ(phase delay between adjacent elements) = ±120° @ 29 GHz [29]. (c) Measured insertion loss in each half structure of three samples of Fig. 5(a). (d) Measured insertion loss in each half structure of three samples of Fig. 5(b) [29].**

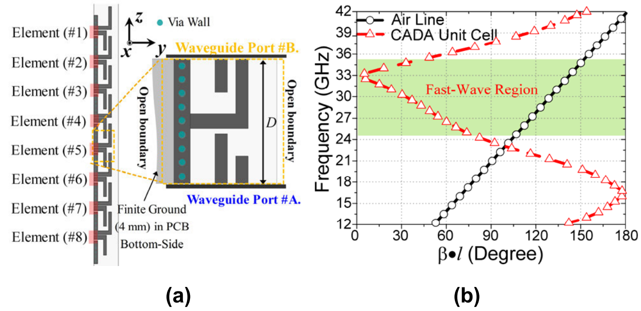

FIGURE 6. **(a) Configuration and simulation setup of the 1-D unit cell to investigate coupling interaction of the proposed CADA(D = 3.6 mm). (b) Dispersion diagram of the proposed CADA unit cell (D = 3.6 mm).**

end-fire direction (+y) in horizontal polarization (E_{theta}-polarization) across the broadband spectrum (25∼35 GHz), as depicted in Figs. 1(c)&2(b)-(c). Moreover, Fig. 1(c) illustrates that the radiation intensity difference toward an end-fire direction (+y) between co-polarization (E_{theta}-polarization) and cross-polarization (E_{phi}-polarization), which is utilized as the radiation performance criterion, is more than 18.0 dB in the frequency range from 25 to 35 GHz [36]. Thus, due to the absence of any auxiliary feeding circuits that can limit antenna performance, the proposed antenna element can achieve high gain toward the end-fire direction (+y) in horizontal polarization across a broadband spectrum.

B. PHASED ARRAY WITH VARIOUS INTER-ELEMENT SPACINGS

To discuss the influence of compression on the proposed CADA in a FR-4 substrate exhibiting highly dielectric lossy media (tanδ: 0.032 @ 28 GHz), the performance of eight elements with three different inter-element spacing (D) is examined (illustrated in Fig. 3) [27]. Meanwhile, 3.6 mm (0.3λ_0) can be regarded as the shortest inter-element spacing within a range with no physical overlap between adjacent elements, and finally causes high mutual coupling. By activating ideally in-phase 50-Ω ports of all elements in ANSYS HFSS simulation, the simulated S-parameters and radiation performance of array antennas with three different spacing are compared in order to investigate the mutual coupling effect, as depicted in Figs. 3-4 [27], [37].

Despite relatively higher mutual coupling levels up to −9.5 dB (average isolation value (S_{ij} @ i=j+1) between each adjacent port) in 3.6 mm spacing, the computed impedance bandwidth is rarely changed as compared with those of the antenna in other spacing, under −10-dB reflection coefficients, in Figs. 3(b)-(c) [27]. In addition, as illustrated in Fig. 3(d), the simulated realized gain toward an end-fire direction (+y) in the eight elements with 3.6 mm spacing is above 7.0 dBi in the operating frequency range from 25 to 35 GHz. Moreover, the proposed 8-element antenna array can exhibit fan-beam characteristics toward the end-fire direction (+y) in Fig. 4. However, due to high mutual coupling effects, some degradation has been observed (e.g., simulated radiation patterns and radiation intensity difference toward end-fire direction (+y) between co-polarization and cross-polarization). Nevertheless, the proposed CADA on a highly dielectric lossy substrate can achieve high gain in broadband without inserting any additional decoupling structures.

Due to the high dielectric loss on an FR-4 substrate, feeding networks in a phased array with three different inter-element spacings should also be designed and characterized, as specifically investigated in [27], [28], [29], and [30]. Fig. 5 depicts the symmetrical configurations of identical T-shaped power dividers in the phased array consisting of three different spacings by integrating grounded coplanar waveguide (GCPW) transmission lines (TL) with via fences for reduction of leakage loss [27], [28], [29]. Moreover, in this paper, the symmetrical configurations of two T-shaped power dividers for boresight and maximum beam steering scenarios have been demonstrated. To estimate the accurate insertion loss of symmetrical configurations with T-shaped power dividers, each 8-section in the back-to-back samples should exhibit

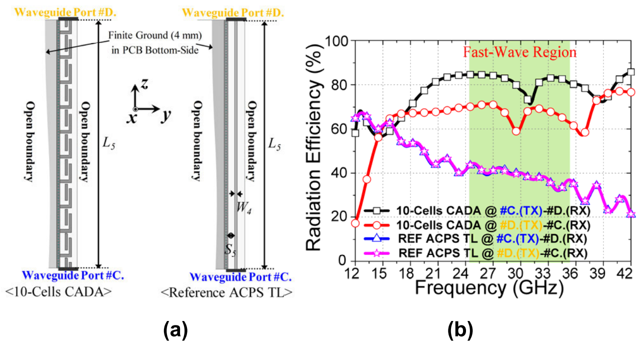

FIGURE 7. (a) Simulation setup method to analyze the radiation coupling interaction of the proposed 10-cell CADA and the reference ACPS TL with identical L_5 (w_4 = 0.36 mm, L_5 = 36 mm, S_5 = 1.04 mm). (b) Simulated radiation efficiency (= leakage power / (leakage power + internal loss)) of the proposed 10-cell CADA and ACPS TL with identical L_5 [28].

constructive interference conditions at a certain frequency (e.g., in-phase difference at 29 GHz as depicted in Figs. 5(a)-(b)) [29], [30], [31]. By measuring back-to-back samples, half of the insertion loss can be regarded as the insertion loss of the feeding networks in the proposed phased array. Figs. 3(c)-(d) presents a small degradation of radiation performance by high mutual coupling of the compressed array configurations. Nevertheless, as illustrated in Figs. 5(c)-(d), all compression feeding networks for boresight and maximum beam steering angle with 3.6 mm spacing exhibit lower insertion loss as compared to other feeding networks.

C. COUPLING MECHANISM VIA LEAKY-WAVE RADIATION BEHAVIOR IN THE PROPOSED 1-D CADA

As already mentioned, the proposed 1-D CADA can become a promising candidate for mm-Wave portable applications due to lots of merits (e.g., low-cost fabrication process, balun-free, and decoupling-free configuration). However, the intrinsic coupling mechanism should be investigated from the point of view of the metamaterial 1-D array concept, as follows [36], [45], [46], [48].

First, to investigate the coupling mechanism in the metamaterial array concept, an adequate unit cell simulation setup is required for 1-D CADA featuring horizontal polarized end-fire radiation. In other words, the longitudinal electric fields-based guided-wave analysis method with two open boundary conditions (+*y*, -*y*) and two waveguide ports assignment (+*z*, -*z*) should be utilized in the proposed 1-D CADA unit cell setup of an asymmetric coplanar strip (ACPS)-based transmission line (TL) [45], [46].

As specifically referred to [36] and [46], the 1-D CADA with 8 elements for the horizontally-polarized end-fire radiation characteristics can be simplified to a unit cell with an ACPS TL type. The modified unit cell of the proposed 1-D CADA consists of an asymmetric radiator and a finite ground plane with the via wall structures [46]. At that time, it can achieve the analysis of an actual radiation mechanism that is similar to the leaky-wave metamaterial array, by omitting any RF feedline, as illustrated in Fig. 6(a) [46]. Because the equivalent circuits of the proposed CADA unit cell within the

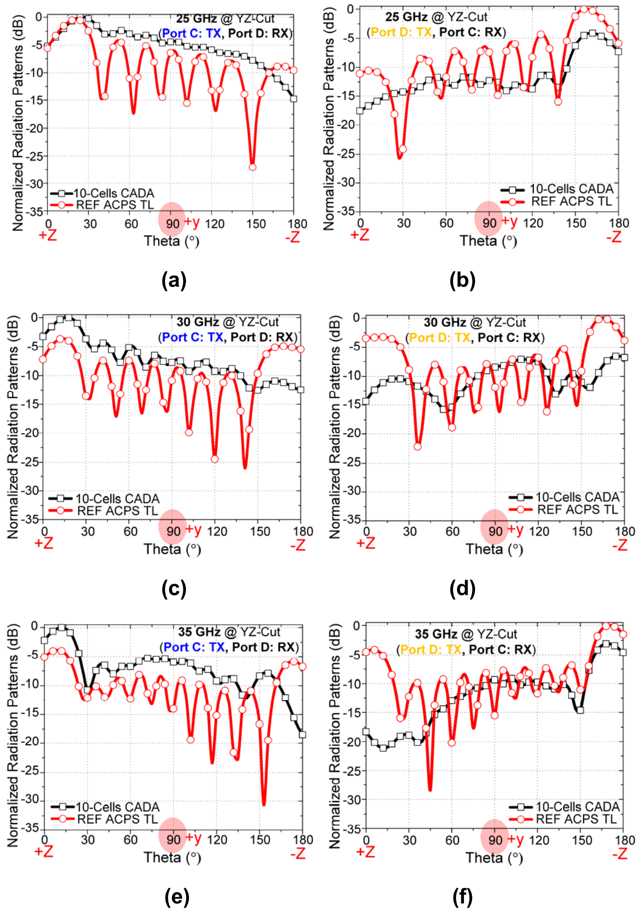

FIGURE 8. Simulated radiation patterns of the proposed 10-cell CADA and the reference ACPS TL with identicalL_5. (a) 25 GHz and Port C(Active.)-Port D(Term.). (b) 25 GHz and Port D(Active.)-Port C(Term.). (c) 30 GHz and Port C(Active.)-Port D(Term.). (d) 30 GHz and Port D(Active.)-Port C(Term.). (e) 35 GHz and Port C(Active.)-Port D(Term.). (f) 35 GHz and Port D(Active.)-Port C(Term).

compact (D = 3.6 mm) spacing are similar to the equivalent metamaterial TL circuit of the conventional TCDA, the dispersion diagram of the unit cell including air-line can be obtained, as illustrated in Fig. 6(b) [43], [44]. Eventually, the desired operating band (25∼35 GHz) of the 1-D CADA unit cell is within the fast-wave region, representing typical leaky-wave behavior. Moreover, the balanced frequency, which can be regarded as the center frequency within the open-stop band, is 32 GHz.

Second, the generalized setup solution for the asymmetric array configuration and special boundary issue is needed to analyze and discuss the detailed coupling interaction in the proposed 1-D CADA. Fig. 7(a) illustrates the simulation method used to analyze typical standing-wave and traveling-wave mechanisms, utilizing the proposed 10-cell CADA and the reference ACPS TL with an identical L_5 (L_5 = 36 mm). At that time, the proposed 10-cell CADA, including two edge dummy elements, can become an adequate setup solution to investigate the coupling interaction of the actual 8-element CADA sample with RF feeding networks in Figs. 9(a)-(b) [45]. Moreover, the impedance of the two waveguide ports

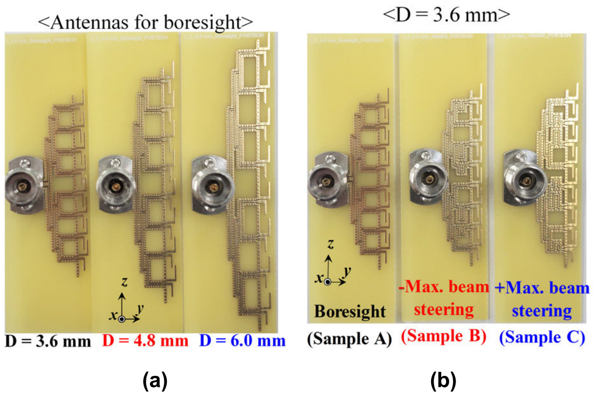

FIGURE 9. (a) Photograph of three samples of the fabricated antennas with different spacing for boresight direction. (b) Photograph of three samples of the fabricated antennas for three different beam directions at $D = 3.6$ mm.

should be identical between the proposed 10-cell CADA and the reference ACPS TL to investigate the coupling interaction during effective radiation between elements, as illustrated in Fig. 7(a). The assigned port impedance of the CADA and the reference ACPS TL is 100-Ω. Therefore, the simulated radiation characteristics (e.g., radiation efficiency and normalized radiation patterns in E-Cut (*yz*-Cut)) between the two configurations can be compared to analyze the coupling mechanism leaky-wave behavior.

As referred to [28], the simulated radiation efficiency can be regarded as the leakage power ratio. Fig. 7(b) illustrates the simulated radiation efficiency of the proposed CADA and the reference ACPS TL by varying the activation and termination setup between two ports. Because the proposed CADA between two ports exhibits an asymmetric structure, the variation of the activation and termination setup should be compared and discussed. The proposed CADA can exhibit a higher leakage power ratio than the reference ACPS TL, and then can achieve the leaky-wave behavior and frequency-selective characteristic in the fast-wave region of Fig. 7(b). Additionally, the typical open-stop band effect near the balanced frequency (32 GHz) of the leaky-wave antenna is observed in the proposed CADA.

Finally, the detailed coupling interaction has been investigated during radiation between elements of the proposed 1-D CADA. The typical leaky-wave antenna can be categorized by the traveling-wave mechanism, and the typical TCDA can also exhibit broadband characteristics featuring high mutual coupling between active elements. In [46], because the ACPS TL-based leaky-wave antenna with a high attenuation constant can achieve a short effective radiation aperture within a smaller number of unit cells, the coupled power level between elements can be exponentially decreased. Apart from the standing-wave mechanism with lots of null points (scan blindness) in radiation patterns, the number of null points of the traveling-wave mechanism can be inherently reduced due to the exponential attenuation constant [45]. Moreover, the proposed 1-D CADA exhibits up to −9.5 dB mutual coupling level, as illustrated in Fig. 3(c). So, Figs. 8(a)-(f) depicts the simulated radiation patterns of the proposed CADA and

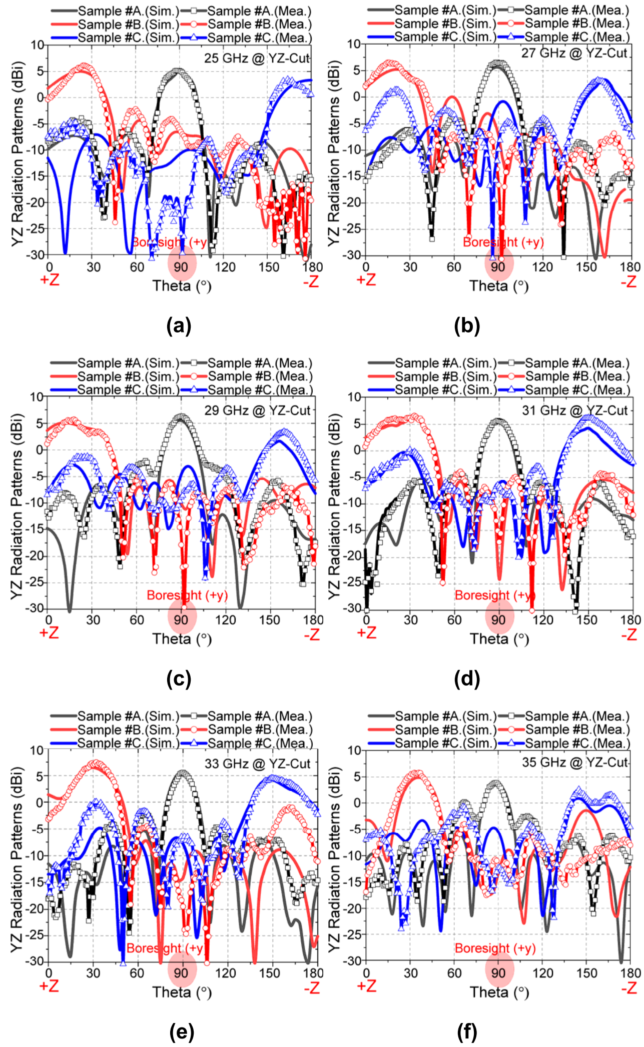

FIGURE 10. Simulated & measured radiation patterns(E_{theta}-pol.) of the fabricated antennas for beam steering test @ $D = 3.6$ mm. (a) 25 GHz. (b) 27 GHz. (c) 29 GHz. (d) 31 GHz. (e) 33 GHz. (f) 35 GHz.

the reference ACPS TL with identical L_5. In conclusion, because the CADA exhibits a gradual attenuation impact and high mutual coupling between elements, each array element consisting of the proposed antenna can be demonstrated for the coupling mechanism via leaky-wave radiation behavior.

III. VERIFICATION RESULTS OF THE PROPOSED ARRAY

This section illustrates and discusses the verification results of the proposed CADA phased array, such as measured radiation performance, simulated total scan pattern and coverage efficiency, measured OTA results, and a comparison table of state-of-the-art antennas featuring fan-beam characteristics toward the end-fire direction in mmWave spectrum.

A. SIMULATED AND MEASURED RADIATION PERFORMANCES

Fig. 9(a) illustrates three samples of the fabricated antennas with different inter-element spacing for boresight direction

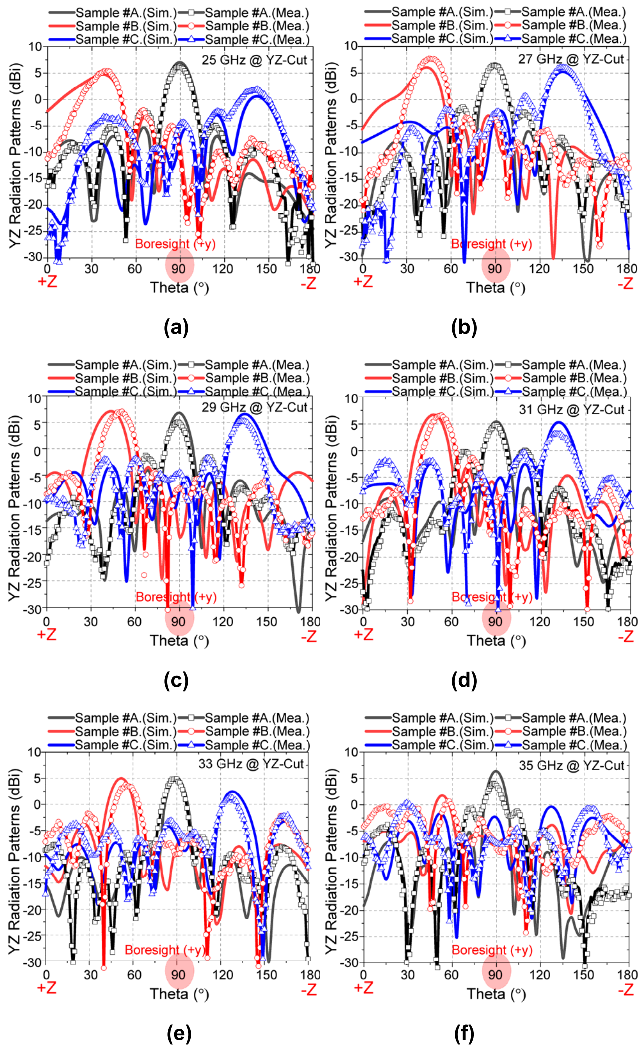

FIGURE 11. Simulated & measured radiation patterns(E_{theta}-pol.) of the fabricated antennas for beam steering test @ $D = 4.8$ mm. (a) 25 GHz. (b) 27 GHz. (c) 29 GHz. (d) 31 GHz. (e) 33 GHz. (f) 35 GHz.

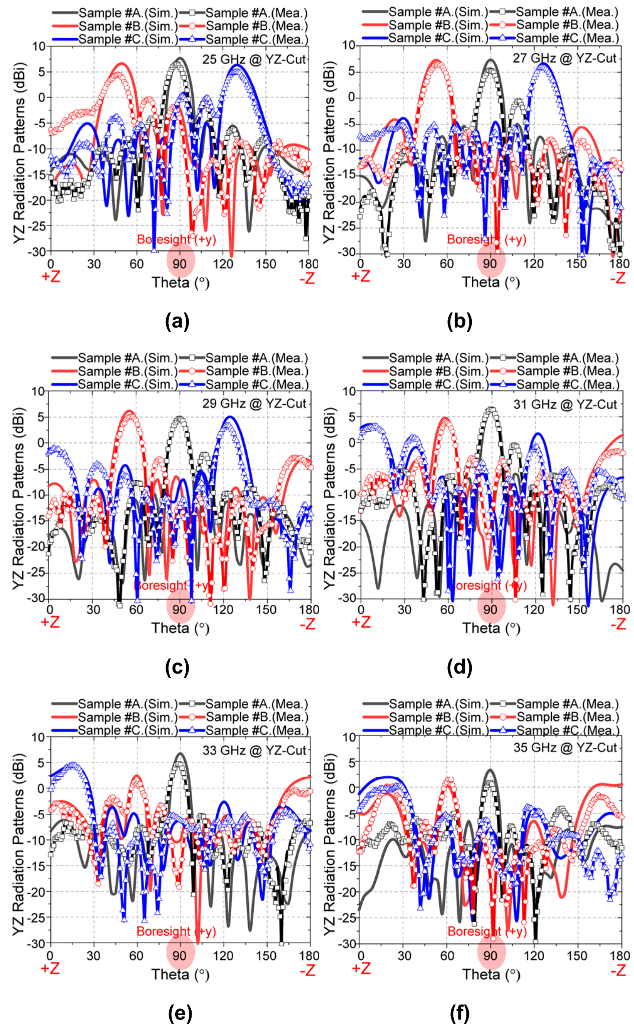

FIGURE 12. Simulated & measured radiation patterns(E_{theta}-pol.) of the fabricated antennas for beam steering test @ $D = 6.0$ mm. (a) 25 GHz. (b) 27 GHz. (c)29 GHz. (d) 31 GHz. (e) 33 GHz. (f) 35 GHz.

integrating 8-element CADA and in-phase power dividers in section II-B and Fig. 5(a). In other words, each antenna has been fabricated by using half of the back-to-back T-junction power dividers with the in-phase difference in Fig. 5(a). Meanwhile, to validate the beam scanning capability, three antenna samples, including power dividers with the pre-determined phased delay for each beam steering direction (boresight ± maximum beam steering angle), have been fabricated as depicted in Fig. 9(b) [27], [28], [29], [47]. In addition, each antenna sample for ± maximum beam steering angle has also been fabricated by using half of the back-to-back T-junction power dividers exhibiting the phased delay (±Δ) in Fig. 5(b) [47].

Figs. 10-12 presents the simulated and measured radiation patterns of the fabricated antennas with different inter-element spacing over a wide frequency range. Within a 3-dB scan loss, the antennas with 3.6 mm spacing exhibit more than 140° (±70°) beam scanning coverage in the frequency range from 25 to 29 GHz and more than 110° (±55°) beam scanning coverage in the frequency range from 31 to 35 GHz. Meanwhile, the maximum scanning coverage of other spacing is narrower than that of 3.6 mm spacing. As depicted in the wide element spacing of Fig. 5, the large phase shift required between adjacent elements in the same beamforming codebook and the increasing insertion loss of the bulky feeding network consequently result in a large beam squint in an operating band [13], [14], [15], [38]. In particular, in Fig. 10(c), 11(c), and 12(c), the maximum beam scanning coverage of the proposed antenna within 3-dB scan loss at 29 GHz carrier frequency can exhibit 140° (±70°), 90° (±45°), and 68° (±34°) at D = 3.6 mm, 4.8 mm, and 6.0 mm, respectively. Thus, the unintended beam squint effect eventually results in narrow beam-scan coverage within a narrow operating band. Moreover, it is ascertained that the presented CADA with a 3.6 mm spacing can achieve a wide-angle scanning capability across the broadband spectrum, rather than other antennas with larger inter-element spacings, as illustrated in the simulation and measurement results of Figs. 10-12.

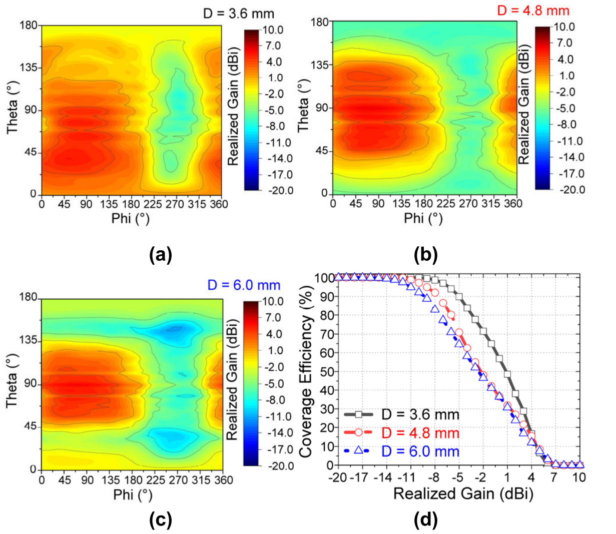

FIGURE 13. Simulated beam scan coverage (average value) of the designed array antennas at 25, 27, 29, 31, 33, and 35 GHz. (a) total scan patterns @ $D = 3.6$ mm. (b) total scan patterns @ $D = 4.8$ mm. (c) total scan patterns @ $D = 6.0$ mm. (d) coverage efficiency vs. realized gain.

B. TOTAL SCAN PATTERN AND COVERAGE EFFICIENCY

To investigate the wide beam scanning characteristics of the proposed CADA despite the single-layer FR-4 PCB process, the total scan patterns (TSPs) and coverage efficiencies over a wide frequency band should be evaluated [19], [27], [28]. As illustrated in Fig. 13, the beam scanning characteristics of the arrays designed with different inter-element spacings have been compared by using the average value of TSPs and coverage efficiencies for frequencies from 25 to 35 GHz.

The proposed CADA with 3.6 mm spacing exhibits quasi-isotropic spherical coverage within the more highly realized gain, despite high mutual coupling between antenna elements due to the compressed configurations. Moreover, it has been ascertained that the compressed array with 3.6 mm spacing could improve the realized gain (at a coverage efficiency of 50%) by more than 3.0 dB, compared to the array with 6.0 mm spacing, between 25 and 35 GHz.

C. MEASURED OTA RESULTS

In this section, the RF signal performance test of the proposed CADA in the practical OTA environment is discussed by varying different modulation schemes, symbol rates, and beam scanning angles to investigate the optimal cell coverage [12], [13]. Representatively, an error vector magnitude (EVM) is one critical factor to discuss regarding the RF signal quality of the proposed CADA containing the 1by8 T-junction power dividers fabricated on a single-layer FR-4 substrate with highly lossy dielectric material [12], [13], [27], [29], [39]. In particular, the CADA with different inter-element spacings utilizing the compression effects in mmWave portable apparatus can be characterized and investigated for fast and precise optimized cell coverage by comparing both measured radiation patterns and over-the-air (OTA) performance results at the same time [12], [13], [29], [39].

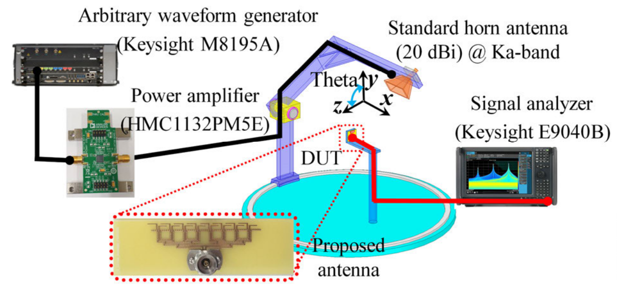

FIGURE 14. EVM measurement setup of the fabricated antennas at 29 GHz.

As depicted in Figs. 14-15, the system performance of several fabricated arrays consisting of different inter-element spacings and passively phased beamforming feeding networks is measured in various OTA environments and characterized. To realize highly effective isotropic radiated power (EIRP) with a good link budget condition at 75 cm of far-field distance during OTA performance tests, a commercial power amplifier (PA) based on a gallium arsenide (GaAs) pseudomorphic high electron mobility transistor (pHEMT) is utilized [40]. At that time, the setup linear gain and carrier frequency of the PA are always fixed at 23 dB and 29 GHz, respectively, due to the utilized operating bandwidth limitation (27∼32 GHz) of the PA. Fig. 15 illustrates the measured EVM versus scan angles or data rates at 29 GHz using six combination examples with different modulation schemes and symbol rates (#1: QPSK and 200 MBaud, #2: 16-QAM and 200 MBaud, #3: 64-QAM and 200 MBaud, #4: 16-QAM and 400 MBaud, #5: 64-QAM and 400 MBaud, #6: 64-QAM and 800 MBaud). When Keysight M8195A arbitrary waveform generator (AWG) is utilized as a TX signal source, the created signal power is fixed to 3.5 dBm.

In Figs. 15(a)-(f), it has been ascertained that the proposed CADA with 3.6 mm inter-element spacing could receive 4.8 Gbps with < 9.0% EVM over a ±70° scan angle range using 64-QAM and 800-MBaud. Moreover, using this modulation method, the array with 3.6 mm inter-element spacing could deliver higher data rates within the lowest and minimized standard deviation EVM compared to the other array configurations, despite its wide scan range. Thus, the measured OTA results exhibit good EVM performance for all modulation schemes with large symbol rates over wide scan ranges as compared to mmWave 3GPP standard specifications [39].

D. COMPARISON OF STATE-OF-THE-ART ANTENNA ARRAYS FEATURING FAN-BEAM RADIATION CHARACTERISTICS TOWARD END-FIRE DIRECTION FOR mmWave PORTABLE APPLICATIONS

Table 1 presents a comparison with state-of-the-art antenna arrays featuring horizontally polarized and fan-beam characteristics toward the end-fire direction for the mmWave portable applications. For the first time, the proposed antenna array demonstrates wide-angle scanning capability over a broadband spectrum. This capability is achieved due to high

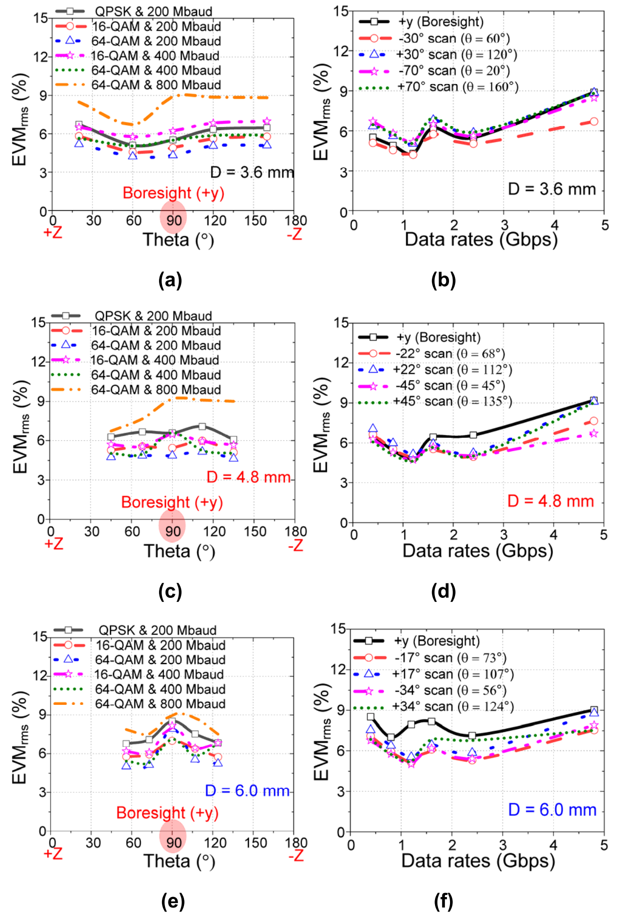

FIGURE 15. Measured OTA results for various inter-element spacing with different modulation formats at 29 GHz. (a) EVM vs. scan angle @ D = 3.6 mm. (b) EVM vs. data rate @ D = 3.6 mm. (c) EVM vs. scan angle @ D = 4.8 mm. (d) EVM vs. data rate @ D = 4.8 mm. (e) EVM vs. scan angle @ D = 6.0 mm. (f) EVM vs. data rate @ D = 6.0 mm.

mutual coupling via leaky-wave behavior between the 1-D linear array elements.

There has been considerable research and literature on the figure of merit (FoM) for phased array antenna design in mmWave portable applications [1], [2], [3], [49]. However, evaluating and standardizing the performance of various fabrication process-based antenna designs remains challenging due to multiple material platforms, design trade-offs, essential antenna parameters, and form factors. Nevertheless, the typical FoM for compact mmWave antennas with hemispherical coverage for portable applications is given by equation (1):

$$FOM_{Ant.} = \frac{\Omega_{scan}}{\Omega_{Half-sphere}} \cdot \frac{\Delta\omega}{\omega_0} \cdot \frac{\lambda_0^3}{Volume} \qquad (1)$$

where $\Omega_{scan}/\Omega_{Half-sphere}$ is the maximum 3-dB beam scanning range divided by half-spherical space at the operating frequency, and $\Delta\omega/\omega_o$ is the fractional operating bandwidth within the 3-dB beam scanning range [49].

Despite the usage of FR-4 PCB process and the compressed configurations without any auxiliary circuits (e.g., balun and decoupling circuits), the proposed antenna arrays can exhibit higher FoM than that compared to state-of-the-art antenna arrays, as presented in Table 1 [19], [20], [28]. In addition, the proposed array using an extremely low-cost fabrication process realizes quasi-isotropic spherical coverage across a broadband spectrum and good EVM performance at high data rates.

TABLE 1. Comparison with the state-of-the-art antenna arrays featuring fan-beam radiation characteristics toward end-fire direction for mmWave portable applications.

	[19]	[20]	[28]	This work
Antenna type (Feeding type)	Two-sided dipole arms (differential stripline without balun)	Tightly coupled dipole (Balun and Wilkinson power divider)	ILA with HIS (T-junction power divider without balun)	Compact and asymmetric dipole (T-junction power divider without balun)
Fabrication process	Multi-layer PCB (Taconic RF-30)	Multi-layer PCB (Taconic RF-35)	Single-layer PCB (FR-4)	Single-layer PCB (FR-4)
Coupling mechanism of a linear array	Surface current reduction via open loop mode	Surface-wave interaction between elements	HIS properties via slow-wave behavior	Traveling-wave mechanism via leaky-wave behavior
Dielectric constant	3	3.5	4.4	4.4
Loss tangent	0.0014	0.0018	0.032	0.032
Antenna Volume (λ_0^3@ center freq.)	0.143	0.137	0.027	0.025
3-dB beam scan range @ operating frequency	≥120° (±60°) @ 25, 27, 29, 31, 33 GHz	≥-30°~0° @ 24 GHz*, ≥-27°~0° @ 28 GHz*	≥ 140° (±70°) @ 26, 28, 30 GHz, ≥110° (±55°) @ 32, 34, 36 GHz,	≥140° (±70°) @ 25, 27, 29 GHz, ≥110° (±55°) @ 31, 33, 35 GHz,
$FoM_{Ant.}$	1.286 (=120/180*8/29*0.143)	0.374 (=60/180*4/26*0.137)	7.301 (=110/180*10/31*0.027)	8.148 (=110/180*10/30*0.025)

*The 3 dB beam scan range in the reference paper are reported about the measured results in only half space of hemispherical area.

IV. CONCLUSION

In this paper, a mmWave CADA based on a single-layer FR-4 PCB for wide-angle scanning capability over a wide bandwidth is proposed and characterized. First, the proposed CADA has been demonstrated to exhibit a high coupling level by a leaky-wave radiation behavior in a 1-D linear array, despite the absence of any balun and decoupling structures. Then, the proposed array can achieve hemispherical beam coverage across a broadband spectrum and good EVM performance, due to the low-loss characteristics of the compressed feeding networks. Thus, due to cost-effective fabrication technology, the presented array can serve as a promising candidate for mmWave 5G global service in mobile devices.

In addition, despite the absence of additional circuits within the compressed configurations, this design methodology can be extended to mmWave on-glass or optically transparent antennas for B5G applications and sub-THz antenna-on-chip (AoC) for 6G applications to realize quasi-spherical coverage of a wide bandwidth [41], [42].

ACKNOWLEDGMENT

The authors are grateful to HANSEM DIGITEC Corporation for their support of sample fabrication. In addition, the ANSYS simulation tool was supported by the ANSYS Corporation.

REFERENCES

[1] Y. Huo, X. Dong, W. Xu, and M. Yuen, "Enabling multi-functional 5G and beyond user equipment: A survey and tutorial," *IEEE Access*, vol. 7, pp. 116975–117008, 2019.
[2] K. Zhao et al., "Spherical coverage characterization of 5G millimeter wave user equipment with 3GPP specifications," *IEEE Access*, vol. 7, pp. 4442–4452, 2019.
[3] S. Ghosh and D. Sen, "An inclusive survey on array antenna design for millimeter-wave communications," *IEEE Access*, vol. 7, pp. 83137–83161, 2019.
[4] K. O. Kenneth et al., "Opening terahertz for everyday applications," *IEEE Commun. Mag.*, vol. 57, no. 8, pp. 70–76, Aug. 2019.
[5] J. Lee, J.-J. Park, K.-W. Kim, H. K. Kwon, and M.-D. Kim, "Measurement-based omnidirectional millimetre-wave and sub-THz propagation analysis in a large cubicle office environment," *IET Microw., Antennas Propag.*, vol. 17, no. 6, pp. 443–453, May 2023.
[6] X. Gu, D. Liu, and B. Sadhu, "Packaging and antenna integration for silicon-based millimeter-wave phased arrays: 5G and beyond," *IEEE J. Microw.*, vol. 1, no. 1, pp. 123–134, Jan. 2021.
[7] Y. Zhang and J. Mao, "An overview of the development of antenna-in-package technology for highly integrated wireless devices," *Proc. IEEE*, vol. 107, no. 11, pp. 2265–2280, Nov. 2019.
[8] A. Alizadeh et al., "Planar 200-GHz transceiver modules," *IEEE J. Solid-State Circuits*, vol. 60, no. 1, pp. 230–243, Jan. 2025.
[9] M. Maggi et al., "Millimeter-wave phased arrays and over-the-air characterization for 5G and beyond: Overview on 5G mm-wave phased arrays and OTA characterization," *IEEE Microw. Mag.*, vol. 23, no. 5, pp. 67–83, May 2022.
[10] A. Lamminen, J. Säily, J. Ala-Laurinaho, J. de Cos, and V. Ermolov, "Patch antenna and antenna array on multilayer high-frequency PCB for D-band," *IEEE Open J. Antennas Propag.*, vol. 1, pp. 396–403, 2020.
[11] S. Y. Lee, D. Lee, Y. Zhang, W. Hong, and N. Ghalichechian, "History and the latest progress in antenna packaging technology: Part 1: Multilayer solutions," *IEEE Antennas Propag. Mag.*, vol. 67, no. 3, pp. 48–61, Jun. 2025.
[12] W. Lee, C. Ozdag, J.-O. Plouchart, A. Valdes-Garcia, and B. Sadhu, "A 24 to 30-GHz phased array transceiver front end with 2.8 to 3.1-dB RX NF and 22 to 24% TX peak efficiency," *IEEE J. Solid-State Circuits*, vol. 59, no. 9, pp. 2788–2804, Sep. 2024.
[13] A. Ahmed, L. Li, M. Jung, S. Li, D. Baltimas, and G. M. Rebeiz, "140-GHz 2-D scalable on-grid 8×8-element transmit–receive phased arrays with up/down converters demonstrating a 5.2-m link at 16 gbps," *IEEE Trans. Microw. Theory Techn.*, vol. 72, no. 5, pp. 2852–2868, May 2024.
[14] B. Yang, Z. Yu, R. Zhang, J. Zhou, and W. Hong, "Local oscillator phase shifting and harmonic mixing-based high-precision phased array for 5G millimeter-wave communications," *IEEE Trans. Microw. Theory Techn.*, vol. 67, no. 7, pp. 3162–3173, Jul. 2019.
[15] F. Xie et al., "A 220-GHz planar triangular lattice transmitter array with 42.7-dBm peak EIRP for long-distance high-data-rate wireless communication," *IEEE Trans. Microw. Theory Techn.*, vol. 73, no. 6, pp. 3194–3208, Jun. 2025.
[16] M. ur Rehman, S. Ravichandran, A. O. Watanabe, S. Erdogan, and M. Swaminathan, "Characterization of ABF/glass/ABF substrates for mmWave applications," *IEEE Trans. Compon., Packag., Manuf. Technol.*, vol. 11, no. 3, pp. 384–394, Mar. 2021.
[17] N. Hiramatsu et al., "Loss evaluation of microstrip line using low-loss olefin-based resin build-up film in 160-GHz band," *IEEE Trans. Microw. Theory Techn.*, vol. 73, no. 9, pp. 5897–5908, Sep. 2025.
[18] W. Hong, K.-H. Baek, and S. Ko, "Millimeter-wave 5G antennas for smartphones: Overview and experimental demonstration," *IEEE Trans. Antennas Propag.*, vol. 65, no. 12, pp. 6250–6261, Dec. 2017.
[19] I. Syrytsin, S. Zhang, G. F. Pedersen, and A. S. Morris, "Compact quad-mode planar phased array with wideband for 5G mobile terminals," *IEEE Trans. Antennas Propag.*, vol. 66, no. 9, pp. 4648–4657, Sep. 2018.
[20] J.-Y. Shim, J.-G. Go, and J.-Y. Chung, "A 1-D tightly coupled dipole array for broadband mmWave communication," *IEEE Access*, vol. 7, pp. 8258–8265, 2019.
[21] M. H. Awida, A. H. Kamel, and A. E. Fathy, "Analysis and design of wide-scan angle wide-band phased arrays of substrate-integrated cavity-backed patches," *IEEE Trans. Antennas Propag.*, vol. 61, no. 6, pp. 3034–3041, Jun. 2013.
[22] L. Zhao, Y. He, G. Zhao, X. Chen, G.-L. Huang, and W. Lin, "Scanning angle extension of a millimeter-wave antenna array using electromagnetic band gap ground," *IEEE Trans. Antennas Propag.*, vol. 70, no. 8, pp. 7264–7269, Aug. 2022.
[23] X. Ding, B.-Z. Wang, and G.-Q. He, "Research on a millimeter-wave phased array with wide-angle scanning performance," *IEEE Trans. Antennas Propag.*, vol. 61, no. 10, pp. 5319–5324, Oct. 2013.
[24] G. Yang, Y. Zhang, and S. Zhang, "Wide-band and wide-angle scanning phased array antenna for mobile communication system," *IEEE Open J. Antennas Propag.*, vol. 2, pp. 203–212, 2021.
[25] B. Xiong, Y. Zhu, Y. Xu, W. Xie, and L. Han, "A novel millimetre-wave 2D wide-angle scanning phased array antenna based on decoupling surface," *IET Microw., Antennas Propag.*, vol. 18, no. 11, pp. 810–818, Nov. 2024.
[26] H. H. Gerami and R. Kazemi, "Development of a compact metasurface antenna with reconfigurable pattern through mode combination technique for 5G mm-wave applications," *IET Microwave Antennas Propag.*, vol. 18, pp. 885–897, 2024.
[27] J.-Y. Lee, J. Choi, D. Choi, Y. Youn, and W. Hong, "Broadband and wide-angle scanning capability in low-coupled mm-wave phased-arrays incorporating ILA with HIS fabricated on FR-4 PCB," *IEEE Trans. Veh. Technol.*, vol. 70, no. 3, pp. 2076–2088, Mar. 2021.
[28] J.-Y. Lee, J. Choi, B. Kim, Y. Oh, and W. Hong, "Performance enhancement of mm-wave phased arrays for mobile terminals through grounded coplanar waveguide feeding networks with via fences," *Frontiers Commun. Netw.*, vol. 2, pp. 1–11, Oct. 2021.
[29] J.-Y. Lee, J. Choi, M. Kim, D. Lee, M. Kim, and W. Hong, "Streamlined millimeter-wave and subterahertz spherical far-field measurement system supporting various antenna types and feed interfaces: Use cases of antenna measurement system," *IEEE Antennas Propag. Mag.*, vol. 66, no. 4, pp. 65–82, Aug. 2024.
[30] J.-Y. Lee et al., "Design and measurement considerations of feeding network including power divider for multi-port antenna arrays," in *Proc. IEEE CAMA*, Oct. 2019, pp. 279–281.
[31] S. M. Moghaddam, J. Yang, and A. U. Zaman, "Fully-planar ultra-wideband tightly-coupled array (FPU-TCA) with integrated feed for wide-scanning millimeter-wave applications," *IEEE Trans. Antennas Propag.*, vol. 68, no. 9, pp. 6591–6601, Sep. 2020.
[32] J. P. Doane, K. Sertel, and J. L. Volakis, "A wideband, wide scanning tightly coupled dipole array with integrated balun (TCDA-IB)," *IEEE Trans. Antennas Propag.*, vol. 61, no. 9, pp. 4538–4548, Sep. 2013.
[33] C.-H. Hu, B.-Z. Wang, R. Wang, S.-Q. Xiao, and X. Ding, "Ultrawideband, wide-angle scanning array with compact, single-layer feeding network," *IEEE Trans. Antennas Propag.*, vol. 68, no. 4, pp. 2788–2796, Apr. 2020.
[34] M. H. Novak, F. A. Miranda, and J. L. Volakis, "Ultra-wideband phased array for small satellite communications," *IET Microw., Antennas Propag.*, vol. 11, no. 9, pp. 1234–1240, Jul. 2017.
[35] W. Hu et al., "Wideband circularly polarized antenna using single-arm coupled asymmetric dipoles," *IEEE Trans. Antennas Propag.*, vol. 68, no. 7, pp. 5104–5113, Jul. 2020.
[36] J.-Y. Lee, J. Choi, J.-H. Jang, and W. Hong, "Performance enhancement in compact inverted-L antenna by using 1-D EBG ground structures and beam directors," *IEEE Access*, vol. 7, pp. 93264–93274, 2019.
[37] *ANSYS Electronics HFSS: 3D High Frequency Simulation Software*, ANSYS Corporation, 2021.
[38] V. Raghavan, M.-L. Chi, M. A. Tassoudji, O. H. Koymen, and J. Li, "Antenna placement and performance tradeoffs with hand blockage in millimeter wave systems," *IEEE Trans. Commun.*, vol. 67, no. 4, pp. 3082–3096, Apr. 2019.
[39] *3GPP, Technical Specification Group Radio Access Network*, document TR 38.817-01 V 16.1.0, 2019. [Online]. Available: https://portal.3gpp.org/desktopmodules/Specifications/SpecificationDetails.aspx?specificationId=3359

[40] (2018). *HMC1132PM5E GaAs PHEMT MMIC Power Amplifier From 27 GHz To 32 GHz*. [Online]. Available: https://www.analog.com/media/en/technical-documentation/data-sheets/HMC1132PM5E.pdf

[41] Z. J. Silva, C. R. Valenta, and G. D. Durgin, "Optically transparent antennas: A survey of transparent microwave conductor performance and applications," *IEEE Antennas Propag. Mag.*, vol. 63, no. 1, pp. 27–39, Feb. 2021.

[42] H. M. Cheema and A. Shamim, "The last barrier: On-chip antennas," *IEEE Microw. Mag.*, vol. 14, no. 1, pp. 79–91, Jan. 2013.

[43] J. L. Volakis and K. Sertel, "Narrowband and wideband metamaterial antennas based on degenerate band edge and magnetic photonic crystals," *Proc. IEEE*, vol. 99, no. 10, pp. 1732–1745, Oct. 2011.

[44] M. O. Anastasiadis, C. L. Zekios, S. B. Venkatakrishnan, and J. L. Volakis, "A comprehensive review on tightly coupled dipole arrays," *IEEE Trans. Antennas Propag.*, vol. 74, no. 5, pp. 3819–3834, May 2026.

[45] H. Koo and S. Nam, "Mechanism and elimination of scan blindness in a T-printed dipole array," *IEEE Trans. Antennas Propag.*, vol. 68, no. 1, pp. 242–253, Jan. 2020.

[46] M. Kim et al., "Antenna-on-display concept on an extremely thin substrate for sub-6 GHz wireless applications," *IEEE Trans. Antennas Propag.*, vol. 70, no. 7, pp. 5929–5934, Jul. 2022.

[47] P.-Y. Feng, S.-W. Qu, S. Yang, L. Shen, and J. Zhao, "Ku-band transmitarrays with improved feed mechanism," *IEEE Trans. Antennas Propag.*, vol. 66, no. 6, pp. 2883–2891, Jun. 2018.

[48] J.-Y. Lee, T. Kim, and W. Hong, "Compact and asymmetric dipole antenna array exhibiting high mutual coupling via leaky-wave radiation behavior," in *Proc. 56th EuMC*, 2026, submitted for publication.

[49] H. Zhang and A. Shamim, "Wideband and wide beam scanning dual-polarized phased array antenna-in-package design for 5G applications," *IEEE Open J. Antennas Propag.*, vol. 5, pp. 140–152, 2024.

JAE-YEONG LEE (Member, IEEE) received the B.S. and M.S. degrees in wireless communications engineering from Kwangwoon University, Seoul, South Korea, in 2008 and 2010, respectively, and the Ph.D. degree from Gwangju Institute of Science and Technology (GIST), Gwangju, South Korea, in 2018.

In 2018, he joined Pohang University of Science and Technology (POSTECH), South Korea, as a Post-Doctoral Fellow, and a Research Assistant Professor with the Microwave, Antenna, Device and System (MADs) Laboratory. He is currently a Senior Researcher with the X-ray·Terahertz Components and Research Section, Electronics and Telecommunications Research Institute (ETRI), Daejeon, South Korea. He has been involved on more than 15 national research projects. He has authored or co-authored 17 peer-reviewed journals and 49 conferences papers, and invented four granted patents. His research interests include metamaterial-based microwave/mmWave/THz antennas and massive MIMO array module fully integrating with mmWave/THz optoelectronic IC chipsets. He has served as a Technical Program Committee Member for the International Symposium on Antennas and Propagation (ISAP), Incheon, South Korea, in 2024. During the IEEE International Symposium on Antennas and Propagation and USNC-URSI Radio Science Meeting (AP-S-USNC-URSI) 2023 and ISAP 2024, he was served as a Special Session Organizer.

SHUAI ZHANG (Fellow, IEEE) received the B.E. degree from the University of Electronic Science and Technology of China, Chengdu, China, in 2007, and the Ph.D. degree in electromagnetic engineering from the Royal Institute of Technology (KTH), Stockholm, Sweden, in 2013.

In 2014, he joined Aalborg University, Denmark, where he is currently a Full Professor and the Head of Antenna Research Group. In 2010 and 2011, he was a Visiting Researcher at Lund University, Sweden, and Sony Mobile Communications AB, Sweden, respectively. He was also an External Antenna Specialist at Bang and Olufsen, Denmark, from 2016 to 2017. He has supervised/co-supervised ten post-doctorals and 18 Ph.D. students. He has co-authored more than 150 articles in well-reputed international journals and more than 17 U.S. or WO patents. His citations in Scopus are more than 7200 with an H-index of 44. His current research interests include millimeter-wave antennas for cellular communications, bioelectromagnetics, metasurfaces, CubeSat antennas, massive MIMO antennas, wireless sensors, and RFID antennas. He was a recipient of the IEEE Antennas and Propagation Society Young Professional Ambassador in 2022. He has been intensively invited to international conference and industry to give keynote/plenary speech and presentations. Since 2024, he has been European Association on Antennas and Propagation (EurAAP) Regional Delegate. He is an Associate Editor of IEEE ANTENNAS AND WIRELESS PROPAGATION LETTERS and *IET Microwaves, Antennas and Propagation*. He is the General Co-Chair of iWAT2023 at Aalborg, Denmark, and a TPC or meta reviewer for several top IEEE conferences.

WONBIN HONG (Fellow, IEEE) is currently a Chaired Professor with Pohang University of Science and Technology (POSTECH), South Korea. He is also the Co-Founder and the Co-CEO of Kreemo Inc. He is one of the first researchers to pioneer the concept and design of millimeter-wave antennas and RF front ends for cellular antenna-in-package (AiP) in the field of consumer electronics, including mobile terminals and access points for the much-anticipated ultrafast broadband wireless solutions, such as 5G/6G and SATCOM. He is also an inventor of Antenna-on-Display (AoD) Technology. He has authored and co-authored more than 250 peer-reviewed journal articles, conference papers, two book chapters, and one book. He is the inventor of more than 110 granted and 250 pending patents. He has been involved in more than 100 government and industry research projects and currently serves as a technical consultant to numerous multinational tech firms and government agencies.

Dr. Hong is a member of the Young Korea Academy of Science and Technology. His students have received recognition, including the Student Best Paper Award during 2024 IEEE European Conference on Antennas and Propagation (EuCAP), the Best Paper Award during 2025 International Symposium on Antennas and Propagation (ISAP 2025), the First Prize Best Industry Paper and First Prize Best Antenna Measurement Paper during 2024 International Symposium on Antennas and Propagation (ISAP), the First Prize Best Student Paper Award, the Second Prize Best Paper Award during 2023 IEEE International Workshop on Antenna Technologies (iWAT), the Second Place Best Student Paper Award in the 2021 IEEE AP-S Symposium on Antennas and Propagation (AP-S URSI), the First Place Best Student Paper Award in the 2020 IEEE AP-S Symposium on Antennas and Propagation (AP-S URSI), the Best Student Paper Award IEEE European Conference on Antennas and Propagation 2020 (EuCAP), the First Prize Best Student Paper Award in 2018 International Symposium on Antennas and Propagation (ISAP), the 2021 IT Award to the most Outstanding Doctorate Student of POSTECH, the 2022, 2020, 2018 Outstanding Master's Student, Electrical Engineering Department of POSTECH, the Silver Prize, the Gold Prize Award in 2025, the 2023 Samsung Humantech Paper Award, and the Silver Medal in the 14th Samsung ElectroMechanics Best Paper Award 2018. He was a recipient of the 29th Young Engineer Award from the National Academy of Korea in 2025.